Am J Physiol Endocrinol Metab 306: E1–E13, 2014.
First published October 3, 2013; doi:10.1152/ajpendo.00146.2013.

Mitochondrial fragmentation impairs insulin-dependent glucose uptake by modulating Akt activity through mitochondrial Ca^{2+} uptake

Andrea del Campo,[1] Valentina Parra,[1,3] César Vásquez-Trincado,[1] Tomás Gutiérrez,[1] Pablo E. Morales,[1] Camila López-Crisosto,[1] Roberto Bravo-Sagua,[1] Mario F. Navarro-Marquez,[1] Hugo E. Verdejo,[1] Ariel Contreras-Ferrat,[1] Rodrigo Troncoso,[1] Mario Chiong,[1] and Sergio Lavandero[1,2,3]

[1]*Advanced Center for Chronic Diseases (ACCDiS)-CEMC, Facultad Ciencias Químicas y Farmacéuticas y Facultad Medicina, Santiago, Chile;* [2]*Programa de Biología Celular y Molecular, Instituto de Ciencias Biomédicas, Facultad de Medicina, Universidad de Chile, Santiago, Chile; and* [3]*Department of Internal Medicine-Cardiology, University of Texas Southwestern Medical Center, Dallas, Texas*

Submitted 13 March 2013; accepted in final form 28 September 2013

del Campo A, Parra V, Vásquez-Trincado C, Gutiérrez T, Morales PE, López-Crisosto C, Bravo-Sagua R, Navarro-Marquez MF, Verdejo HE, Contreras-Ferrat A, Troncoso R, Chiong M, Lavandero S. Mitochondrial fragmentation impairs insulin-dependent glucose uptake by modulating Akt activity through mitochondrial Ca^{2+} uptake. *Am J Physiol Endocrinol Metab* 306: E1–E13, 2014. First published October 3, 2013; doi:10.1152/ajpendo.00146.2013.—Insulin is a major regulator of glucose metabolism, stimulating its mitochondrial oxidation in skeletal muscle cells. Mitochondria are dynamic organelles that can undergo structural remodeling in order to cope with these ever-changing metabolic demands. However, the process by which mitochondrial morphology impacts insulin signaling in the skeletal muscle cells remains uncertain. To address this question, we silenced the mitochondrial fusion proteins Mfn2 and Opa1 and assessed insulin-dependent responses in L6 rat skeletal muscle cells. We found that mitochondrial fragmentation attenuates insulin-stimulated Akt phosphorylation, glucose uptake and cell respiratory rate. Importantly, we found that insulin induces a transient rise in mitochondrial Ca^{2+} uptake, which was attenuated by silencing Opa1 or Mfn2. Moreover, treatment with Ruthenium red, an inhibitor of mitochondrial Ca^{2+} uptake, impairs Akt signaling without affecting mitochondrial dynamics. All together, these results suggest that control of mitochondrial Ca^{2+} uptake by mitochondrial morphology is a key event for insulin-induced glucose uptake.

mitochondrial fragmentation; Mfn2; Opa1; calcium; insulin

MITOCHONDRIA ARE MULTIFUNCTIONAL ORGANELLES essential for skeletal muscle cell function, as they supply energy for contraction in the form of ATP via oxidative phosphorylation. These organelles form a dynamic network governed by well-ordered processes of biogenesis, degradation, movement along cytoskeleton tubules, and fusion/fission events. Mitochondrial fusion is controlled by the large GTPases optic atrophy 1 (Opa1) and mitofusins 1 and 2 (Mfn1/2), which drive the fusion of the inner and outer membranes between two individual mitochondria. In contrast, mitochondrial fission is controlled by dynamin-related protein-1 (Drp1) and fission protein-1 (Fis1). Fis1 localizes at the mitochondrial surface, where it recruits cytoplasmic Drp1 under fission-promoting stimuli (34). Drp1, in turn, forms a ring that constricts mitochondria, thus generating two daughter mitochondria. Altered levels of these mitochondria-shaping proteins have been reported in several pathologies. Mutations in *mfn2* and *opa1* have been associated with Charcot-Marie-Tooth neuropathy type 2A (1) and with dominant autosomal optic atrophy (3), respectively. Furthermore, decreased levels of Mfn2 and significantly smaller mitochondria have been found in skeletal muscle biopsies of obese and type 2 diabetic patients (17, 37).

Besides its role in mitochondrial morphology, Mfn2 controls apposition between the endoplasmic reticulum (ER) and mitochondria. De Brito and Scorrano showed that Mfn2 is enriched at the ER-mitochondria interphase, and its ablation disrupts interorganelle contacts and reduces the efficiency of ER-mitochondrial Ca^{2+} transfer (14). In the mitochondrial matrix, Ca^{2+} activates three key enzymes of the TCA cycle, pyruvate, α-ketoglutarate, and isocitrate dehydrogenases, therefore stimulating mitochondrial oxidative phosphorylation (10). Furthermore, previous work from our laboratory showed that insulin-induced Akt activation and glucose transporter 4 (GLUT4) traffic to the cell surface requires a rise in intracellular Ca^{2+} levels in cultured cardiomyocytes (12).

A recent study showed that Mfn2 regulates insulin signaling and glucose homeostasis in skeletal muscle by coordinating both mitochondrial and ER functions (30). However, it remains unknown whether mitochondrial morphology itself controls the actions of insulin on glucose homeostasis. To address this question, we investigated the effects of Mfn2 and Opa1 silencing on insulin-induced glucose uptake, mitochondrial function, and mitochondrial Ca^{2+} uptake in L6 rat skeletal muscle cells. Our results show that mitochondrial fragmentation elicited by Mfn2 and Opa1 silencing decreases insulin-dependent glucose uptake, Akt signaling, and cellular oxygen consumption. Importantly, we found that insulin increases mitochondrial Ca^{2+} uptake, which is prevented by Opa1 or Mfn2 silencing. Moreover, treatment with Ruthenium red (RuRed), an inhibitor of mitochondrial Ca^{2+} uptake, also impairs Akt signaling without affecting mitochondrial morphology. Taken together, these results suggest that regulation of mitochondrial Ca^{2+} uptake by mitochondrial morphology is a key event for proper insulin signaling.

MATERIALS AND METHODS

Reagents. Antibodies against Mfn2, Opa1 (polyclonal and monoclonal) and Parkin were from Abcam (Cambridge, MA). Drp1 antibody was from BD Transduction Laboratories (San Jose, CA). PINK1, CHOP, phospho-JNK, JNK, and BIP antibodies were from Santa Cruz Biotechnology (Dallas, TX). Phospho-Akt, Akt, phospho-IRS-1, IRS-1, and phospho-insulin receptor (phospho-IR) antibodies were from Cell Signaling (Danvers, MA). HERP antibody was from

Address for reprint requests and other correspondence: S. Lavandero, Advanced Center for Chronic Diseases (ACCDiS), Facultad Ciencias Químicas y Farmacéuticas & Facultad Medicina, Universidad de Chile, Olivos 1007, Santiago 8380492, Chile (e-mail: slavander@uchile.cl).

BIOMOL Research Laboratories (Plymouth Meeting, PA), and mtHsp70 antibody was from Affinity BioReagents (Glosen, CO). Tetramethylrhodamine methyl ester (TMRM), dihydrorhodamine 123, MitoTracker green and MitoTracker orange were from Invitrogen (Eugene, OR). Cytochalasin B and 2-deoxy-D-glucose were from Calbiochem (La Jolla, CA). Protein assay reagents were from Bio-Rad (Hercules, CA). Insulin, anti-GAPDH antibody, α-MEM, carbonyl cyanide *m*-chlorophenylhydrazone (CCCP), and all other reagents were from Sigma-Aldrich (St. Louis, MO). Generation and use of adenoviruses coding for LacZ, the dominant negative form of Drp1

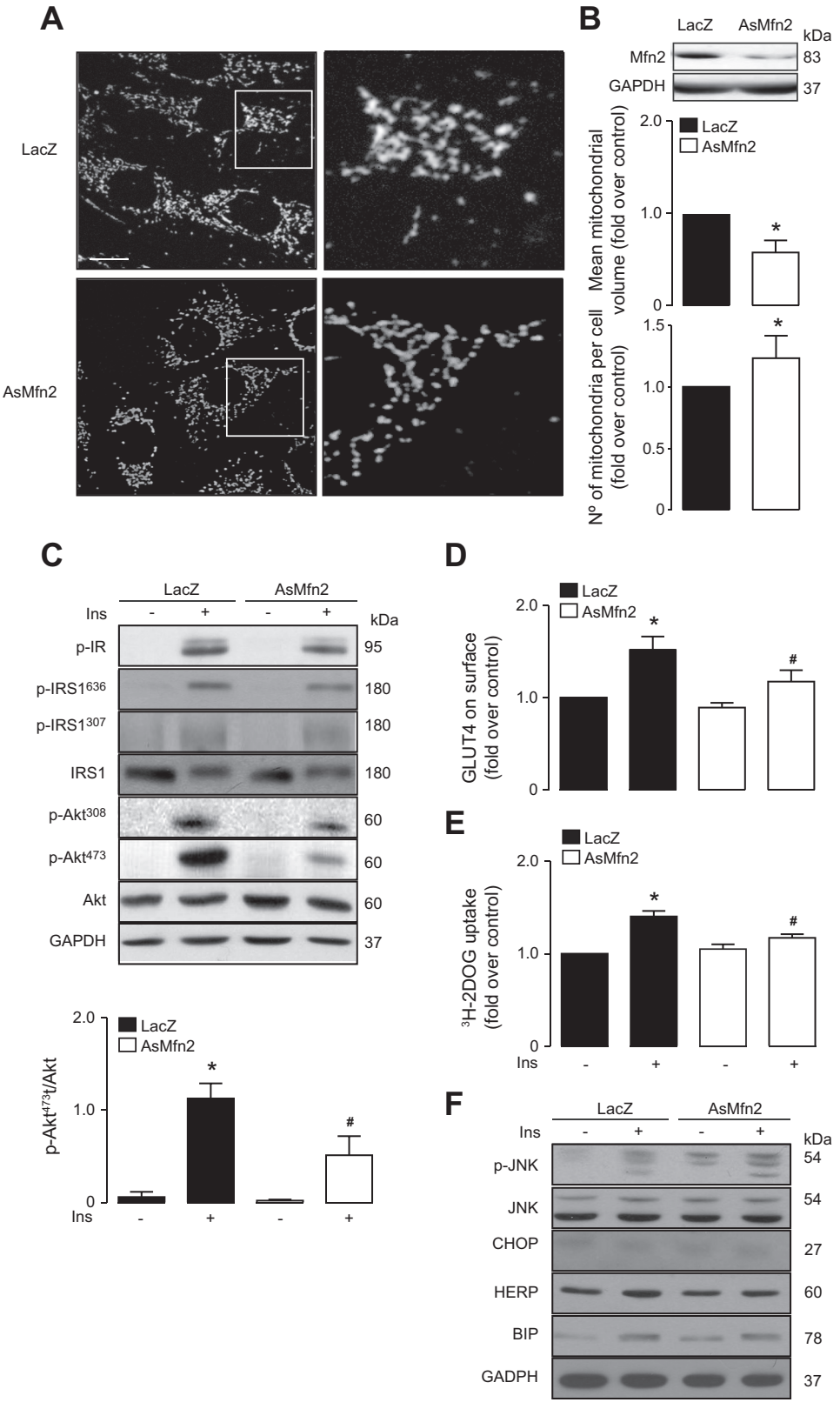

Fig. 1. Mitofusin 2 (Mfn2) silencing causes mitochondrial fission and reduced response to insulin in skeletal muscle L6 myoblasts. *A*: confocal images of the mitochondrial network of cells stained with MitoTracker green. *Right*: ×5 magnification of selected areas; scale bar, = 10 μm. *B*, *top*: Western blot analysis of Mfn2 in AsMfn2 and LacZ cells; *bottom*: quantification of mean volume and number of individual mitochondria per cell ($n = 3$). *C, top:* Western blot analysis of insulin-signaling proteins in LacZ- and AsMfn2-transduced L6-GLUT4myc (c-myc epitope-tagged GLUT4-expressing) cells; *bottom*: quantification of Akt phosphorylation at Ser^{473} ($n = 4$). *D*: quantification of GLUT4myc exposition at the cell surface in response to insulin ($n = 6$). *E*: quantification of glucose uptake of LacZ and AsMfn2 cells in response to 30 min of insulin stimulation ($n = 6$). *F*: representative images of Western blot analysis of markers of endoplasmic reticulum (ER) stress in the different conditions evaluated. All values are expressed as means ± SE. $^*P < 0.05$ vs. LacZ; $\#P < 0.05$ vs. LacZ + Ins.

(Drp1K38A), antisense sequence against Mfn2 (AsMfn2), and miRNA against Opa1 (miOpa1) and miRNA control (miControl) have been described previously (2).

Cell culture. L6 muscle cells expressing c-myc epitope-tagged GLUT4 (GLUT4myc) were cultured as a myoblast monolayer as previously described (18). For all experiments, cells were seeded in 10% FBS-α-MEM for 2 days. At that point, cells were transduced with adenoviral vectors according to experimental group. Cells were maintained in 2% FBS-α-MEM for the next 2 days. For experimentation, cells were maintained in serum-free α-MEM for 3 h and then were exposed to insulin for 0.5 h (100 nM) or left untreated.

Adenoviral transduction. Myoblasts were serum deprived and infected with adenoviral vectors coding for LacZ, Drp1K38A, AsMfn2, miOpa1, or miControl at a multiplicity of infection of 5,000. After 5 h, medium was replaced with 2% FBS-α-MEM.

Western blot. Equal amounts of protein from complete cell extracts were separated by SDS-PAGE (10% polyacrylamide gels) and electrotransferred to nitrocellulose. Membranes were blocked with 5% milk-TBS-T. Membranes were incubated with primary antibodies at 4°C and blotted with horseradish peroxidase-linked secondary antibodies [1:5,000 in 1% (wt/vol) milk in TBS-T]. Signals were detected using ECL (Promega) and quantified by scanning densitometry. Protein content was normalized with GAPDH or β-tubulin.

Mitochondrial morphology. Cells were incubated with 400 nM MitoTracker green or 400 nM MitoTracker orange in Krebs solution for 30 min. Confocal image stacks of the mitochondrial network were captured with a Zeiss LSM 5 Pascal/Axiovert 200 microscope, using a Plan-Apochromat 63x/1.4 oil DIC objective, as described elsewhere (25). Z-stacks were deconvolved, thresholded, and 3D-reconstructed using ImageJ software (NIH). Number and volume of individual mitochondria were quantified using the 3D Object Counter plug-in. Each experiment was repeated at least three times, and 16–25 cells per condition were quantified.

Mitochondrial Ca^{+2} uptake. To determine mitochondrial Ca^{+2} levels, time-lapse images were obtained from cultured GLUT4myc cells preloaded with Rhod2-FF using a Zeiss LSM 5 Pascal/Axiovert 200 microscope, as previously described (32).

Mitochondrial content, transmembrane potential (ψmt), and ROS production. Myoblasts were loaded with 200 nM MitoTracker orange, 200 nM TMRM (23), or 25 nM dihydrorhodamine 123 (22), respectively, for 30 min. Fluorescence was determined by flow cytometry using a FACScan system (Becton-Dickinson).

ATP measurement. Intracellular ATP content was determined using a Cell Titer-Glow Luminescent Cell Viability Assay (Promega) following the manufacturer's instructions. Signals were measured in a TopCount NXT microplate luminescence counter (PerkinElmer) (32).

Respiration rate. Cells were plated on 100-mm dishes, and when they reached confluence, the cells were treated according to experimental design. After trypsinization, oxygen levels of the cell suspension in PBS were measured polarographically at 25°C using a #5331

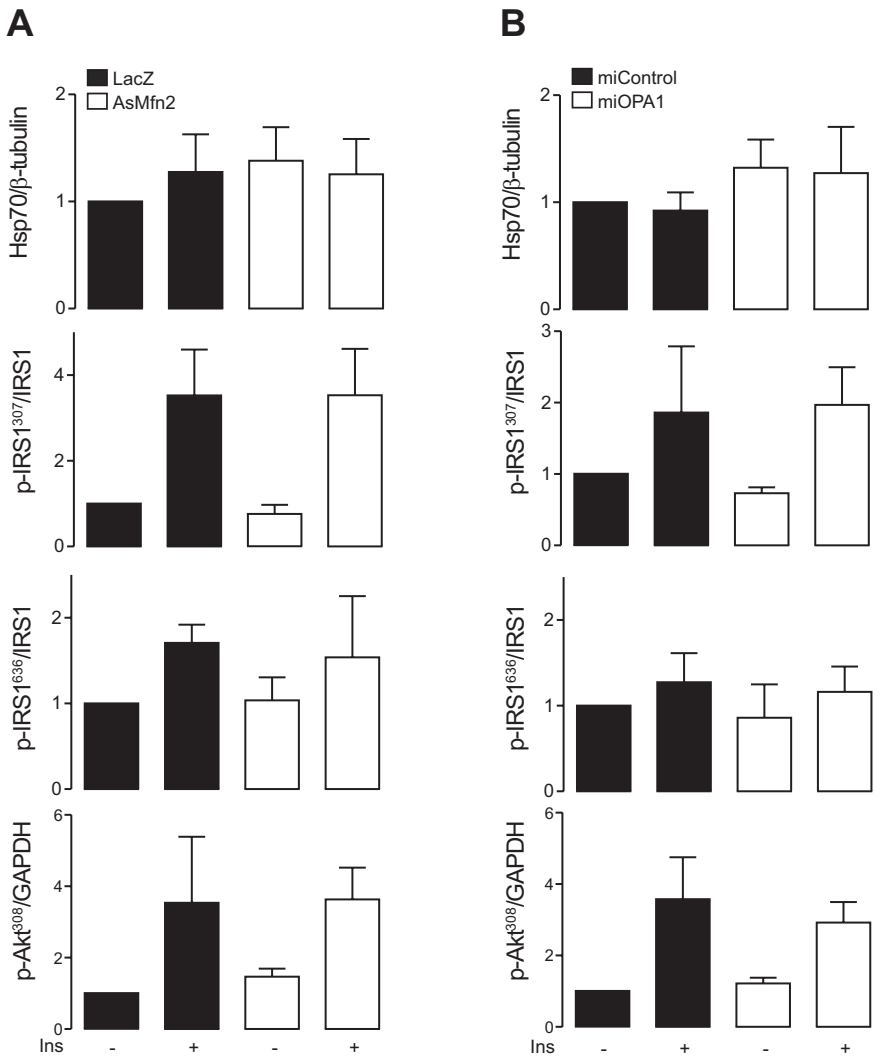

Fig. 2. Quantification of insulin signaling. *A*: quantification of Western blot analysis for Hsp70 ($n = 4$), p-IRS Ser^{307} ($n = 4$), p-IRS Ser^{636} ($n = 4$), and p-Akt Thr^{308} ($n = 3$) in response to insulin treatment for LacZ- and AsMfn2-transduced cells. *B*: quantification of Western blot analysis for Hsp70 ($n = 4$), p-IRS Ser^{307} ($n = 4$), p-IRS Ser^{636} ($n = 4$), and p-Akt Thr^{308} ($n = 3$) in response to insulin treatment for miOpa1- and miControl-transduced cells.

Clark electrode (Yellow Springs Instruments) (8, 32). Maximal oxygen consumption was assessed by uncoupling the respiratory chain with 200 nM CCCP. Respiration rate was determined by the ratio between basal oxygen consumption and maximal oxygen consumption.

2-Deoxy-D-[^{3}H]glucose uptake. Glucose uptake was measured at room temperature for 5 min in transport buffer [20 mM HEPES, pH 7.4, and 10 μM 2-deoxy-D-[^{3}H]glucose (1 mCi/ml)] as described elsewhere (12).

Surface GLUT4myc. Surface myc-tagged GLUT4 was measured as previously reported (36). Briefly, L6-GLUT4myc cells were fixed in 3% paraformaldehyde PBS for 3 min at room temperature and then blocked with 3% BSA 10% goat serum-PBS at 4°C for 30 min. Primary anti-c-myc antibody was incubated at a 1:100 dilution for 60 min at 4°C, followed by incubation with peroxidase-conjugated secondary antibody. One milliliter of OPD reagent (51.4 mM Na_2HPO_4, 24.3 mM citric acid) was added to each well. The colorimetric reaction was stopped by addition of 0.25 ml of 3 N HCl for 10 min at room temperature. The supernatant was collected, and absorbance was measured at 492 nm.

Immunofluorescence and colocalization analysis. Cells were incubated for 30 min with Lysotracker red (LSTR, 100 nM) and MitoTracker green (MTG, 400 nM) and maintained in Krebs solution. Confocal images were captured with a Leica TCS SP5 confocal microscope using a Plan-Apochromat 63x/1.4 oil DIC objective. For colocalization analysis, only one focal plane was analyzed. Images were deconvolved, and the background was subtracted using ImageJ software (NIH). Signal colocalization was quantified using Manders' algorithm, as previously described (25).

Statistical analysis. Data are means ± SE of the indicated sample size (n). Student's t-test was performed for comparisons between two groups. Multiple groups were analyzed using one-way ANOVA followed by a protected Tukey's test. Statistical significance was defined as $P < 0.05$.

RESULTS

Mfn2 knockdown impairs insulin-induced mitochondrial metabolic stimulation. First, the impact of Mfn2 silencing on mitochondrial morphology in L6-GLUT4myc cells was assessed. Mean volume and number of individual mitochondria per cell were quantified via confocal microscopy and 3D reconstruction of the mitochondrial network. AsMfn2 significantly decreased Mfn2 protein levels compared with cells transduced with LacZ. As expected for the silencing of a fusion protein, this intervention lead to mitochondrial fragmentation observed as a decreased mitochondrial mean volume (55%, $P < 0.001$) and increased number of mitochondria per cell (25%, $P < 0.001$) (Fig. 1, *A* and *B*).

Then, we assessed the effect of Mfn2 silencing on insulin signaling. Compared with LacZ cells, AsMfn2 caused a significant decrease in insulin-stimulated Akt phosphorylation at Ser^{473} (55%, $P = 0.001$), without affecting the phosphoryla-

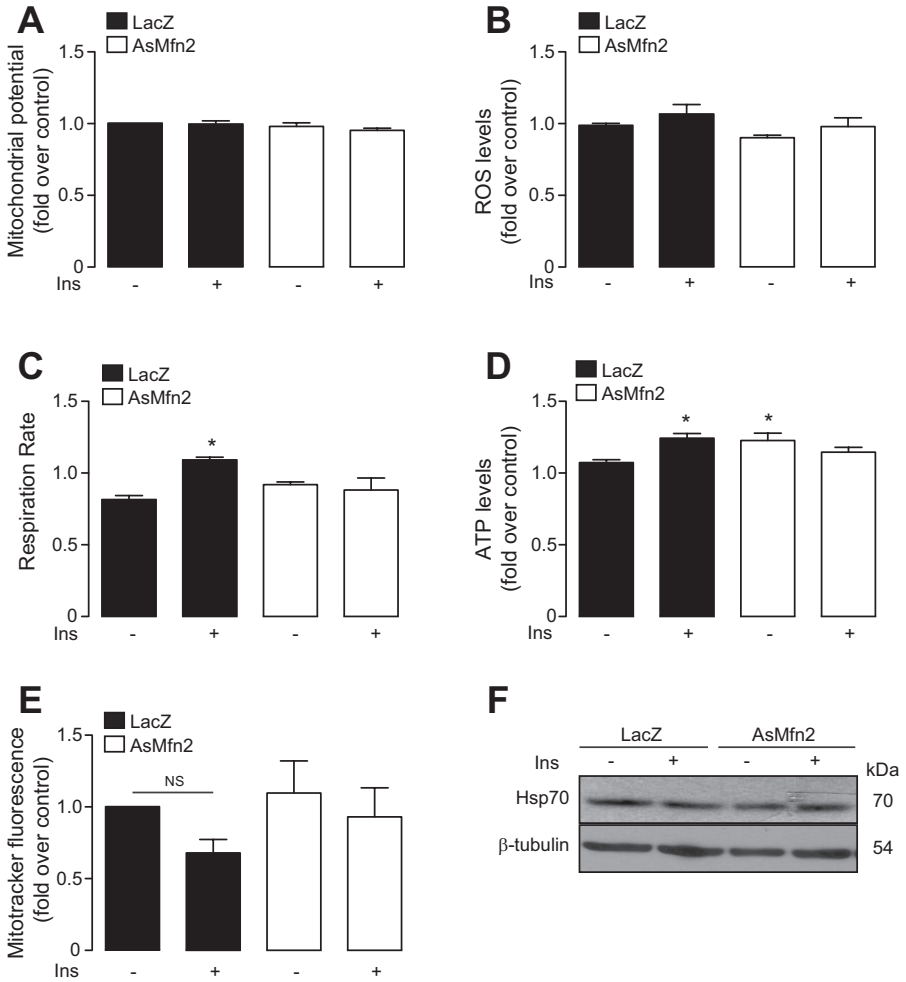

Fig. 3. Mfn2 reduction impairs insulin-induced mitochondrial metabolic stimulation. *A*: mitochondrial potential quantification of LacZ (black) and AsMfn2 (white) cells in response to insulin ($n = 5$). *B*: reactive oxygen species (ROS) production in the different experimental conditions ($n = 4$). *C*: measurement of mitochondrial respiration measured as oxygen consumption rate in response to insulin in LacZ and Mfn2 cells ($n = 5$). *D*: total ATP production for all above-mentioned conditions ($n = 5$). *E*: quantification of mitochondrial content for the different conditions measured as MitoTracker orange incorporation ($n = 3$). *F*: representative image of Western blot analysis of mtHsp70 ($n = 4$). All values are expressed as means ± SE. *$P < 0.05$ vs. LacZ.

tion of IR or IRS-1 in its inhibitory residues Ser^{636} (substrate of mTORC1) and Ser^{307} (substrate of JNK). Moreover, AsMfn2 did not affect Thr^{308}-Akt phosphorylation (Figs. 1*C* and 2*A*). In addition, AsMfn2 significantly diminished both GLUT4 migration to the plasma membrane (26%, $P = 0.003$) and glucose uptake (basal 0.79 ± 0.22; insulin 0.89 ± 0.23 pmol [^{3}H]2-DOG/μg protein) (20%, $P < 0.001$) in response to insulin compared with LacZ (basal 0.74 ± 0.19; insulin 1.01 ± 0.26 pmol [^{3}H]2-DOG/μg protein) (Fig. 1, *D* and *E*). Thus, these data suggest that AsMfn2 silencing disrupts insulin signaling at the Akt level without affecting the upstream IR-IRS1 axis.

Previous reports on Mfn2 participation in insulin resistance indicate that its absence impairs insulin signaling through ER stress (24, 30). Our results showed no evidence of ER stress-mediated disruption of the insulin pathway. In this regard, JNK phosphorylation was increased in AsMfn2-trasduced cells. Nevertheless, this effect appears to be UPR independent, as ER stress markers CHOP, BIP, and HERP remained unchanged between adenoviral treatments (Fig. 1*F*). This observation suggests that Mfn2 modulates Akt through a mechanism different from the UPR. This discrepancy with the aforementioned studies can be explained by the use of different strate-

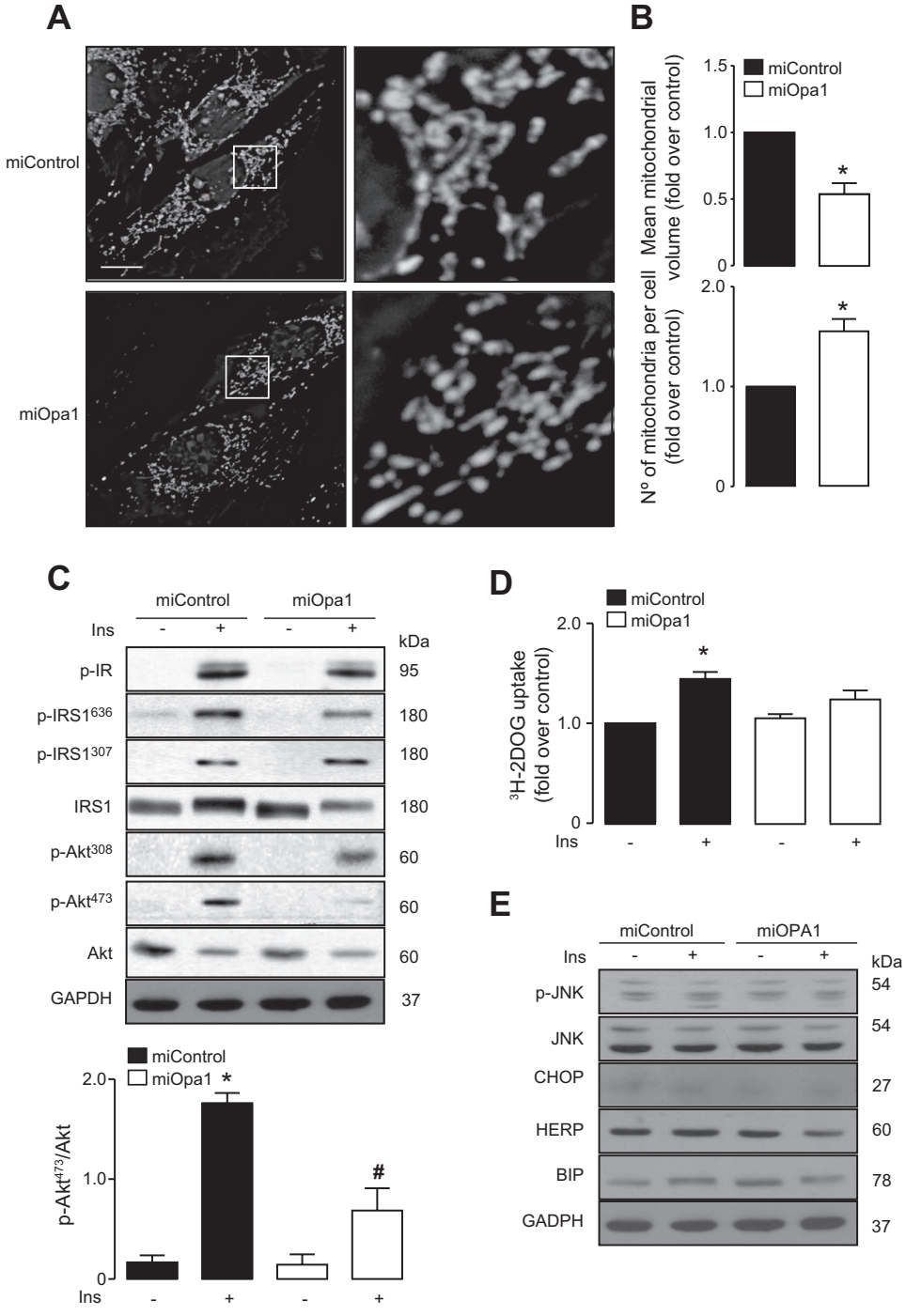

Fig. 4. Diminished levels of optic atrophy 1 (Opa1) cause mitochondrial fission and reduced response to insulin. *A*: confocal images of miControl- and miOpa1-transduced cells stained with MitoTracker orange. *Right*: ×5 magnification of selected areas; scale bar, 10 μm. *B*: quantification of mean volume and number of individual mitochondria per cell ($n = 3$). *C, top*: Western blot analysis of insulin-signaling protein in miControl- and miOpa1-transduced L6-GLUT4myc cells; *bottom*: quantification of Akt phosphorylation at Ser^{473} ($n = 4$). *D*: quantification of glucose uptake in response to 30 min of insulin stimulation ($n = 6$). *E*: Western blot analysis of markers of ER stress in the different conditions evaluated ($n = 4$). All values are expressed as means ± SE. *$P < 0.05$ vs. miRNA control; #$P < 0.05$ vs. miRNA control + Ins.

gies to ablate Mfn2. Our results show cellular response to partial and acute Mfn2 reduction instead of long-term ablation. Of note, insulin stimulation caused increases in BIP levels, JNK phosphorylation, and IRS-1 phosphorylation at Ser^{307} compared with nonstimulated cells (Figs. 1*F* and 2*A*). This insulin-induced mild stress response has been described as an adaptive mechanism to cope with insulin's anabolic effect (26).

Additionally, the impact of Mfn2 silencing on mitochondrial metabolism in response to insulin was studied. The results showed that mitochondrial potential was not altered by insulin or the adenoviral transduction ($P = 0.314$; Fig. 3*A*). Moreover, insulin promoted an increase in ROS production that was not modified by the adenoviral transduction (Fig. 3*B*). Along with maintaining mitochondrial potential, insulin stimulation promoted an increase in ATP production in control cells that was significantly reduced in AsMfn2-transduced cells after insulin stimulation ($P < 0.05$). In contrast, while in a basal state, transduced cells showed a significant increase, likely due to an increase in oxygen-independent ATP production (Fig. 3*D*). Moreover, the increased respiration rate stimulated by insulin (≈8%, $P = 0.03$) in LacZ cells was significantly abolished in AsMfn2-transduced cells (Fig. 3*C*). All of these metabolic effects were due to changes in mitochondrial function rather than fluctuations in mitochondrial content, as two markers of mitochondrial mass, MitoTracker orange and mtHsp70, did not significantly change between conditions (Fig. 3, *E* and *F*).

Opa1 knockdown replicates Mfn2 knockdown effects on insulin signaling. To assess whether our results were due to changes in mitochondrial morphology or the absence of Mfn2 in particular, Opa1 was silenced using miOpa1. This strategy promotes mitochondrial fragmentation independent of Mfn2 level. The results showed a decrease in mean mitochondrial volume (50%, $P < 0.001$) and augmented mitochondrial number per cell (40%, $P < 0.001$) to an extent similar to that achieved with AsMfn2 (Fig. 4, *A* and *B*). Similar to the results with AsMfn2, this impaired mitochondrial fusion significantly decreased Ser^{473} Akt phosphorylation after insulin stimulation (60%, $P < 0.001$), without affecting Akt Thr^{308}, IRS1 Ser^{636}, IRS Ser^{307}, or IR phosphorylation (Figs. 4*C* and 2*B*). As expected, Opa1 silencing also diminished insulin-induced glucose uptake (basal 0.41 ± 0.28; insulin 0.56 ± 0.23 pmol ^{3}H-2DOG/μg protein) compared with miControl (basal 0.52 ± 0.22; insulin 0.89 ± 0.33 pmol [^{3}H]2-DOG/μg protein; Fig. 4*D*). Also similar to AsMfn2, there was no increase in ER stress markers (Fig. 4*E*). Of note, there are several types of glucose transporter, and basal control of glucose uptake is mediated by GLUT1 in muscle cells, which is mainly localized in the plasma membrane. In contrast, GLUT4 is mainly localized in intracellular reservoirs, and after insulin stimulation it is transported to the plasma membrane to increase glucose uptake (28). Mfn2 and Opa1 silencing resulted in no change in basal glucose uptake but reduced insulin-dependent glucose uptake.

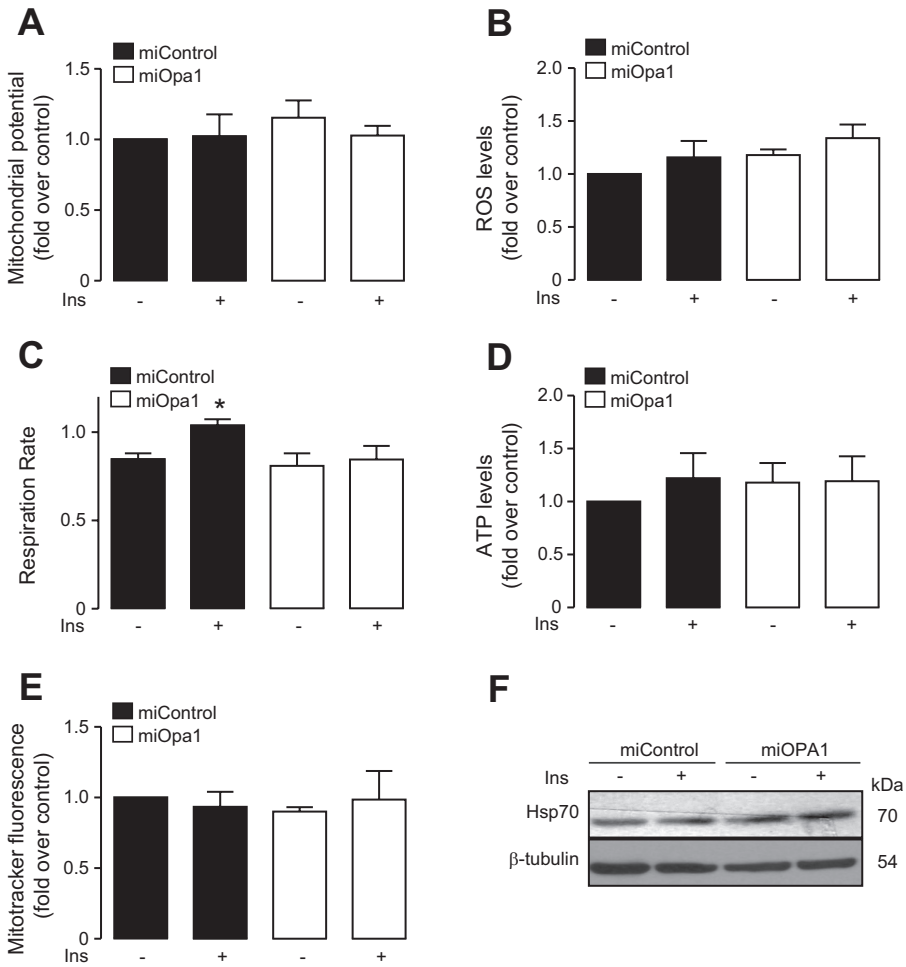

Fig. 5. Opa1 silencing abolishes mitochondrial stimulation elicited by insulin. *A*: mitochondrial potential quantification of miControl- and miOpa1-transduced cells ($n = 5$). *B*: ROS production in response to insulin ($n = 4$). *C*: quantification of oxygen consumption rate for the 4 indicated conditions ($n = 5$). *D*: quantification of ATP levels ($n = 5$). *E*: quantification of mitochondrial content for the different conditions, measured as MitoTracker orange incorporation ($n = 3$). *F*: Western blot analysis of mtHsp70 ($n = 4$). All values are expressed as means ± SE. *$P < 0.05$ vs. miRNA control.

The results of the present work suggest that mitochondrial morphology may mainly affect the inducible glucose uptake mediated by the insulin-Akt-GLUT4 axis.

At a metabolic level, miOpa1 produced the same effects as AsMfn2 (Fig. 5). In particular, mitochondrial potential did not vary after transduction or insulin stimulation (Fig. 5*A*); moreover, ROS production caused by insulin stimulation did not differ between miOpa1- and miControl-transduced cells (Fig. 5*B*). To determine the mitochondrial metabolism, respiratory rate was measured. miControl cells showed a significantly increased respiratory rate in response to insulin, whereas miOpa1-transduced cells did not increase in respiratory rate after insulin stimulation (Fig. 5*C*). In addition to respiratory rate, we measured ATP production. In miRNA-treated cells, no significant changes were observed after insulin stimulation (Fig. 5*D*). MitoTracker orange and mtHsp70 did not differ significantly between conditions (Fig. 5, *E* and *F*). All together, these results suggest that defective mitochondrial fusion directly affects Akt activation upon insulin stimulation.

Drp1 loss-of-function does not affect insulin signaling. Next, to assess the role of the opposite effects on mitochondrial morphology, an adenoviral vector coding for a dominant negative Drp1 (Drp1K38A) was used. Displacement of the mitochondrial balance toward elongation was observed, as well as increased mean mitochondrial volume (90%, $P < 0.001$), concomitant with decreased numbers of mitochondria per cell (30%, $P < 0.001$; Fig. 6, *A* and *B*). Drp1K38A did not affect insulin signaling. The elongated phenotype did not alter insulin-induced Akt Ser^{473} phosphorylation (Fig. 6*C*), nor did it affect GLUT4 traffic to the surface (Fig. 6*D*). In addition, Drp1K38A did not change glucose uptake (basal 1.02 ± 0.50, insulin 1.35 ± 0.68 pmol [^{3}H]2-DOG/μg protein; 20%, $P < 0.001$) compared with LacZ (basal 1.12 ± 0.60, insulin 1.31 ± 0.65 pmol [^{3}H]2-DOG/μg protein; Fig. 6*E*). These data suggest

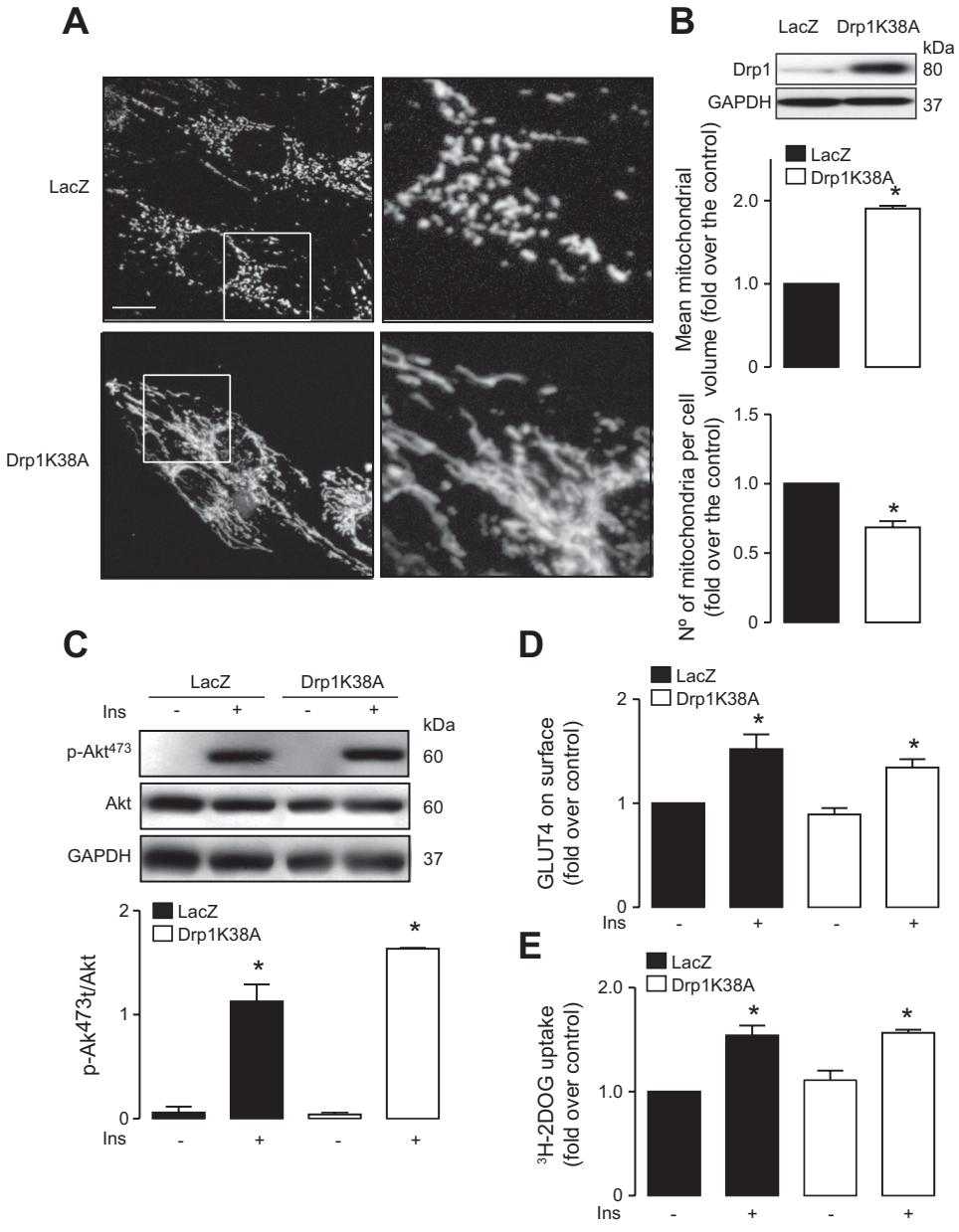

Fig. 6. Decreased fission induced by Drp1K38A (dominant negative form of dynamin-related protein-1) does not affect insulin signaling and effects. *A*: confocal images of LacZ- and Drp1K38A-transduced cells stained with MitoTracker green. *Right*: ×5 magnification of selected area; scale bar, 5 μm. *B*, *top*: Western blot analysis of Drp1 in control and Drp1K38A-transduced cells; *bottom*: quantification of mean volume and number of individual mitochondria per cell ($n = 3$). *C*, *top*: Western blot analysis of Akt phosphorylation at Ser^{473} in LacZ- and Drp1K38A-transduced L6-GLUT4myc cells; *bottom*: quantification of Akt phosphorylation ($n = 4$). *D*: quantification of GLUT4myc exposure at the cell surface in response to insulin ($n = 6$). *E*: quantification of glucose uptake of LacZ and Drp1K38A cells in response to 30 min of insulin stimulation ($n = 6$). All values are expressed as means ± SE. *$P < 0.05$ vs. LacZ.

that mitochondrial network continuity rather than a balance between fusion and fission events is needed for full Akt activation.

Both Mfn2 and Opa1 knockdown disrupt insulin-induced mitochondrial Ca^{2+} uptake. Aside from their role in energy production, mitochondria are also key regulators of Ca^{2+} levels. We addressed whether the morphological changes had repercussions on Ca^{2+} homeostasis and insulin signaling. Our results show that insulin induced an immediate increase in mitochondrial Ca^{2+} uptake, which was completely abolished by the mitochondrial uniporter channel inhibitor RuRed (Fig. 7*A*). Moreover, mitochondrial fragmentation induced by AsMfn2 produced a significant reduction in mitochondrial Ca^{2+} uptake (Fig. 7*B*), probably due to diminished connectivity within the mitochondrial network and decreased contact with the ER. As with AsMfn2, miOpa1 decreased mitochondrial Ca^{2+} uptake (Fig. 7*C*). The reduced Ca^{2+} uptake exerted by imbalanced mitochondrial fragmentation could account for the inability of AsMfn2- and miOpa1-treated cells to increase their metabolism in response to insulin. Insulin-induced Ca^{2+} entrance to the mitochondrial matrix can boost oxidative catabolism, since it stimulates TCA cycle dehydrogenases (9), therefore fueling the respiratory chain and ATP production, a mechanism that could be impaired due to mitochondrial fragmentation.

The possible mechanism linking mitochondrial fragmentation with diminished Ca^{2+} uptake could be diminished ion diffusion: in a more interconnected network, Ca^{2+} enters the

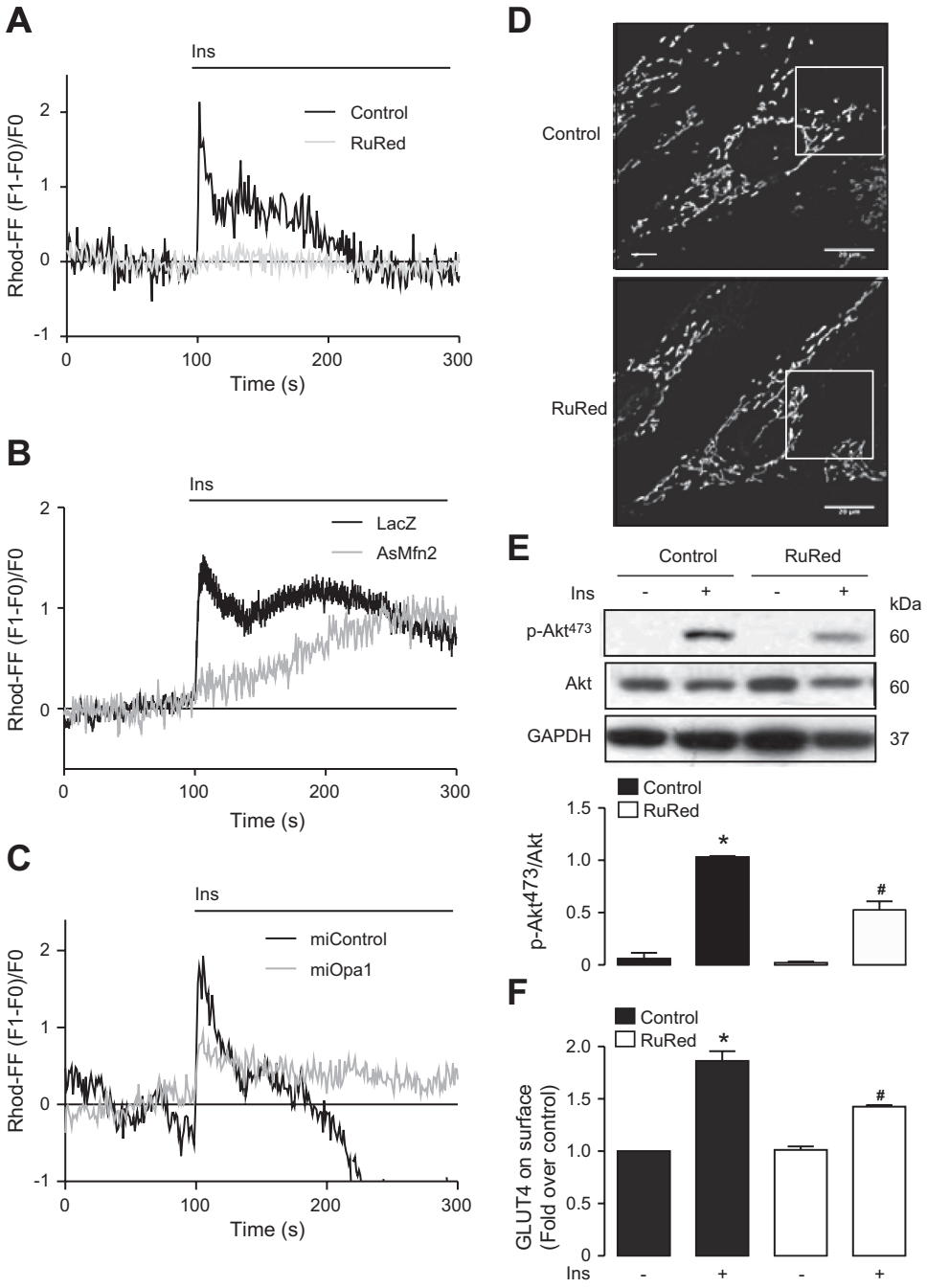

Fig. 7. Decreased levels of Mfn2 or Opa1 impair insulin-induced mitochondrial Ca^{2+} signaling. *A*: changes in mitochondrial Ca^{2+} levels in L6-GLUT4myc cells in response to insulin registered using Rhod-FF ($n = 3$). *B*: insulin-elicited mitochondrial Ca^{2+} signal in LacZ- and AsMfn2-transduced cells. *C*: mitochondrial Ca^{2+} kinetics in miControl- and miOpa1-treated cells. *D*: confocal images of Ruthenium red (RuRed)-treated cells stained with MitoTracker green; scale bar, 10 μm. *E, top*: Western blot analysis of Akt phosphorylation at Ser^{473} in control and RuRed-treated cells; *bottom*: quantification ($n = 4$). *F*: quantification of GLUT4myc exposition at the cell surface of control and RuRed-treated cells in response to insulin ($n = 4$). All values are expressed as means ± SE. *$P < 0.05$ vs. control; #$P < 0.05$ vs. Ins.

mitochondrial matrix and readily diffuses throughout the matrix, allowing for a more efficient uptake. On the other hand, in a fragmented network, diffusion is limited. To gain some insight into the matter, we measured insulin-elicited Ca^{2+} uptake of small and large mitochondria in L6-GLUT4myc cells in basal conditions (Fig. 8, *B* and *C*). Our results show that smaller mitochondria indeed showed a reduced Ca^{2+} uptake, in accord with our proposed mechanism.

Mitochondrial uniporter inhibitor attenuates Akt signaling without interfering with mitochondrial morphology. Since mitochondrial fragmentation reduced mitochondrial Ca^{2+} uptake, we investigated whether impaired Ca^{2+} uptake per se might lead to alterations in insulin signaling or mitochondrial morphology. As shown in Fig. 7*D*, treatment with the mitochondrial uniporter inhibitor RuRed did not affect mitochondrial morphology, since mean volume and number of mitochondria per cell did not differ significantly between conditions (Fig. 8*A*). On the other hand, Akt Ser^{473} phosphorylation and surface GLUT4 levels in response to insulin stimulation were significantly decreased (50%, $P < 0.05$, 50% $P < 0.001$, respectively; Fig. 7, *E* and *F*) in RuRed-treated cells. These results suggest that mitochondrial Ca^{2+} uptake is an important component of insulin signaling and that impaired mitochondrial Ca^{2+} signaling is the mechanism by which mitochondrial fragmentation leads to reduce insulin metabolic response.

DISCUSSION

Different tissues diverge greatly in their mitochondrial organization and in the composition of their respiratory machin-

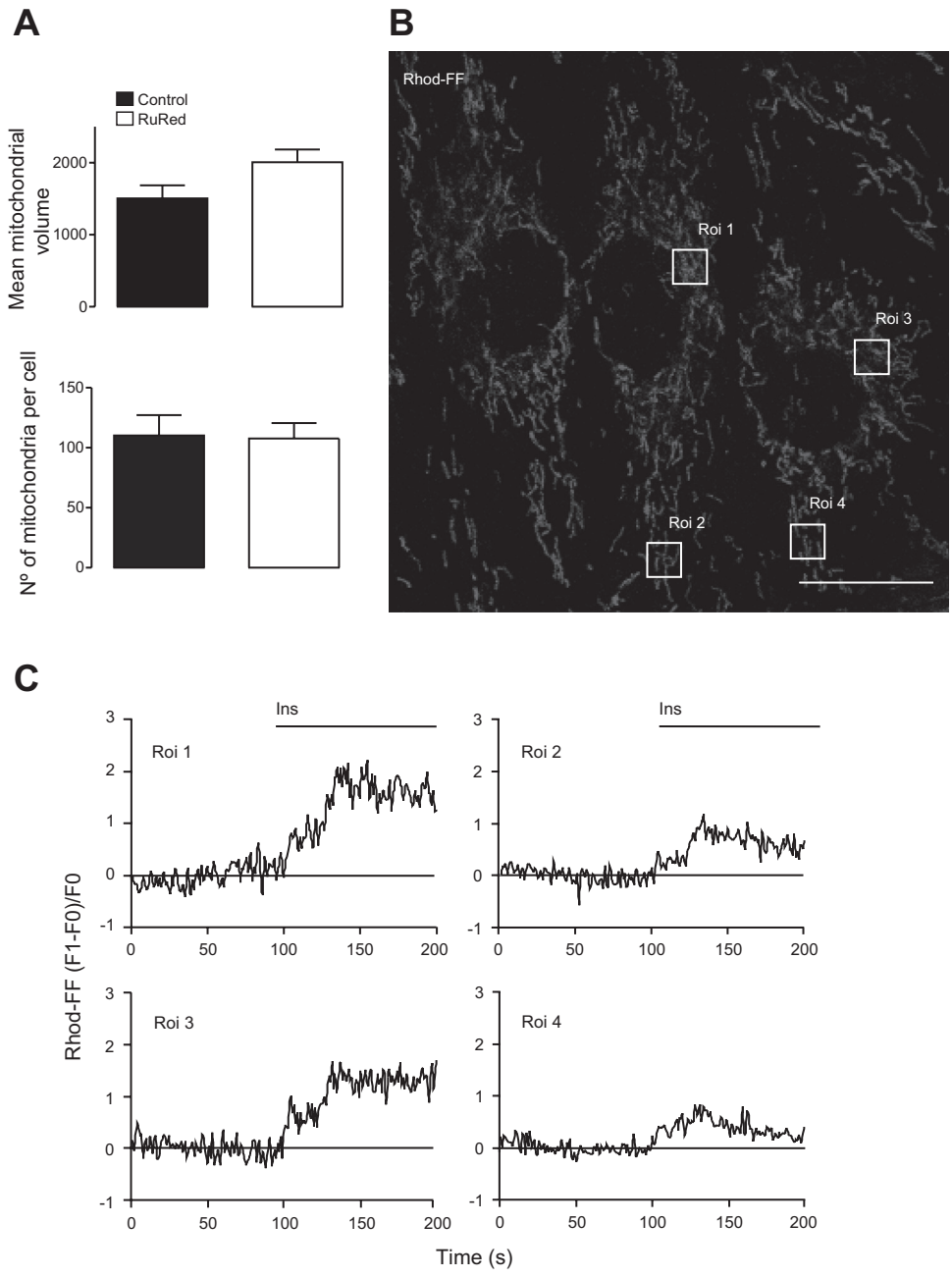

Fig. 8. Ca^{2+} uptake in different-sized mitochondrial populations. *A*: quantification of mean volume and number of individual mitochondria per cell in control and RuRed-treated conditions ($n = 3$). *B*: representative confocal image of L6-GLUT4myc cells loaded with the Ca^{2+}-sensitive dye Rhod-FF; scale bar, 20 μm. *C*: quantification of mitochondrial Ca^{2+} signals in different regions of interest (Roi) comprising both small (Roi 2 and 4) and larger mitochondria (Roi 1 and 3).

ery, as a reflection of specific requirements in physiological or pathological state (5). In tissues with high metabolic rates, mitochondrial network remodeling profoundly affects the function of the respiratory chain, directly impacting cellular metabolism (4). In accordance, both mitochondrial fragmentation and uncoupling of the electron transport chain have been found in the skeletal muscle of obese and diabetic patients (20). Moreover, levels of mitochondria-shaping proteins such as Mfn2, and PARL, a rhomboid-like protease that promotes mitochondrial fusion, are decreased under insulin resistance conditions (35). On this subject, Bach et al. (2) showed that mitochondrial fragmentation induced by Mfn2 silencing leads to metabolic defects such as decreased respiratory rate and glucose oxidation in L6E9 cells. On the basis of these findings, we further proposed a direct relationship between fragmented morphology of the mitochondrial network and disruption of insulin signaling, with a subsequent decrease in glucose utilization in skeletal muscle cells. Our results show that modifying the mitochondrial network by deleting Mfn2 from the system and suppressing fusion alters insulin signaling, along with a significant decrease in GLUT4 traffic, glucose uptake, and mitochondrial metabolism.

Mfn2 silencing dampens insulin signaling, observed as decreased Akt phosphorylation at Ser^{473} without changes in Thr^{308} or its upstream IR-IRS1 axis. Akt Ser^{473} phosphorylation is important for Akt full activation, and is carried out by mTORC2 (29). On the other hand, Akt Thr^{308} is phosphorylated by PDK1, thus underlying control of IR activation. The effects of Mfn2 and Opa1 silencing on Akt phosphorylation sites indicate that mitochondrial morphology is required for insulin signaling, downstream of the IR-IRS1 axis. Recently, it has been reported that mTORC2 partially localizes at the ER-mitochondria interphase within a subdomain termed the mitochondria-associated membranes (MAM), where it interacts with the Ca^{2+} transfer complex IP3R-grp75-VDAC (6). Upon insulin stimulation, mTORC2 is further enriched in the MAM, maintaining its integrity and promoting mitochondrial metabolism through Ca^{2+} uptake. This observation supports mTORC2 as an important regulator of mitochondrial function, as MAM is the platform for its signaling. Interestingly, our present work shows this relationship to be bidirectional, since mitochondrial integrity, in turn, can modulate the insulin-Akt pathway.

Mfn2 fulfills several functions within the cell other than mitochondrial fusion, such as UPR modulation (24), ER-mitochondria tethering (14), and direct regulation of mitochondrial metabolism independently of its mitochondrial fusion activity (31). Such diversity of function renders Mfn2 knock-

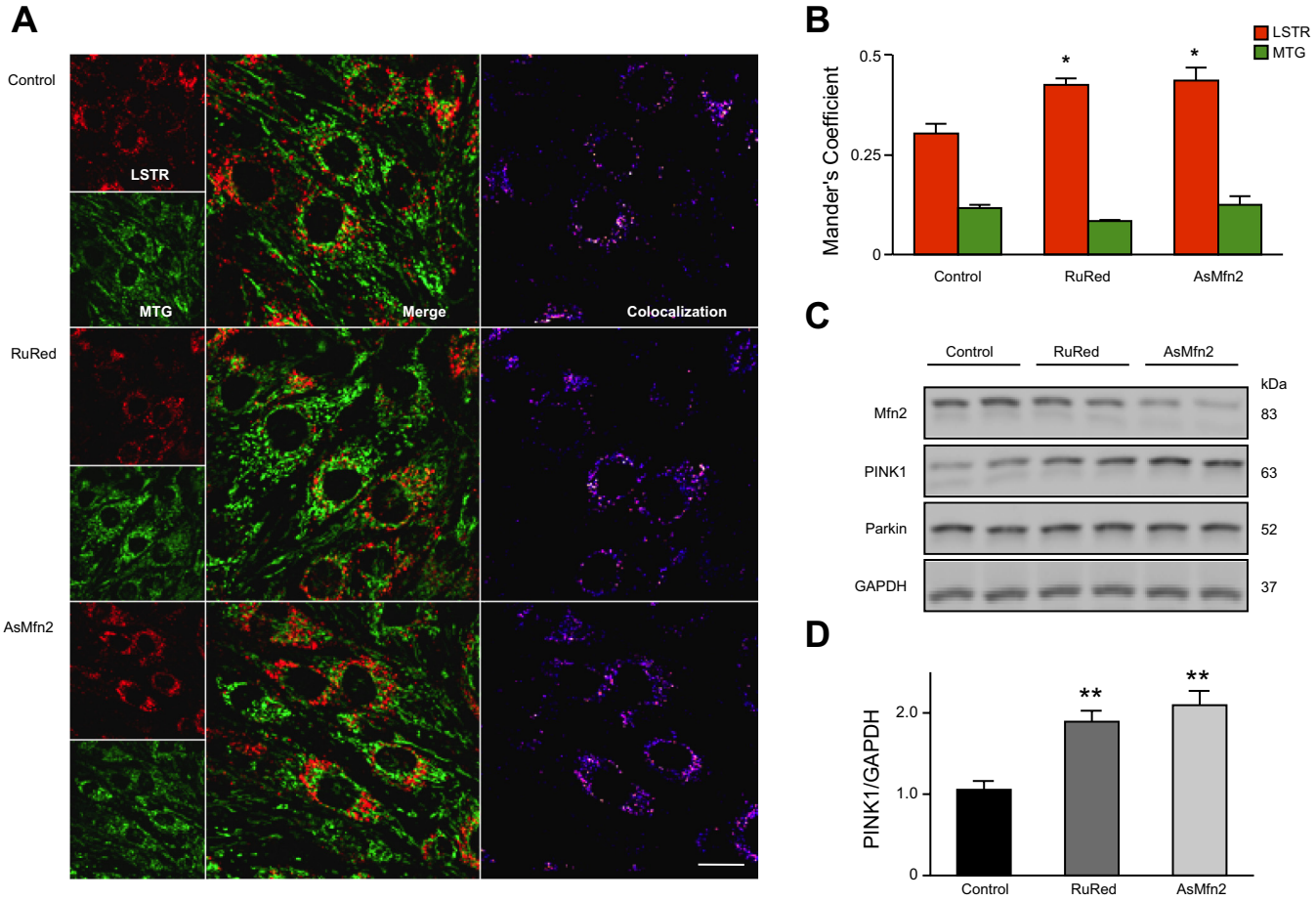

Fig. 9. Effect of mitochondrial Ca^{2+} uptake inhibiton on mitophagy. *A*: confocal images of cells loaded with Lysotracker red (LSTR) and Mitotracker green (MTG) in control, RuRed-treated, or AsMfn2-transduced condition; scale bar, 20 μm. *B*: Manders' coefficients for LSTR and MTG obtained from images as in *A* ($n = 4$). *C*: Western blot analysis of mitophagy-related proteins PINK1 and Parkin in control, RuRed-treated, and AsMfn2-transduced cells. *D*: quantification of PINK1 levels standardized by GAPDH ($n = 4$). All values are expressed as means ± SE. $^*P < 0.05$, $^{**}P < 0.01$ vs. control.

out cells susceptible to great strains, including ER stress, as previously observed (24, 30). Our results do not suggest ER stress, mainly due to the extent of Mfn2 silencing achieved with our strategy. The residual amount of Mfn2 (Fig. 1*B*) allows us to assess the importance of mitochondrial morphology without interference of other perturbations or compensatory processes. Furthermore, to test another method for mitochondrial morphology manipulation, we investigated whether decreased protein levels of Opa1 lead to the same defects as AsMfn2. miOpa1 also downregulated insulin-induced Akt phosphorylation and its associated metabolic boost. Our results support the idea that the fragmented mitochondrial phenotype is responsible for these observations rather than a particular fusion protein.

Opa1 is a highly regulated protein responsible for both the structuring of mitochondrial cristae and the merging of inner membranes during mitochondrial fusion (11). It is regulated, among other mechanisms, through cleavage by intramembrane proteases. Under physiological conditions, effective mitochondrial fusion requires a balance between long and short forms of Opa1. Metabolic alterations promote increased protein cleavage, thus producing a significant increase in short isoforms at the expense of long forms, shifting toward a fragmented organelle morphology (15). Reduced ATP content and dissipation of mitochondrial potential, for example, both lead to Opa1 cleavage by proteases m-AAA and Oma1 (3). Recent literature showed that Opa1 deregulation in Oma1 knockout mice produced insulin resistance, impaired glucose uptake, and unbalanced thermogenesis. Of note, Oma1$^{-/-}$ mice suffer the same effects as individuals fed a high-fat diet, indicating that a balance between long and short forms of Opa1 is required for the maintenance of mitochondrial metabolism (27). All together, these data suggest an important relationship not only between mitochondrial morphology and metabolism but also with insulin resistance. Our results support the idea that Opa1 is a crucial protein in insulin-induced metabolic response.

On the other hand, we tested the opposite scenario by promoting mitochondrial fusion using a dominant negative form of Drp1, Drp1K38A. In this regard, Jheng et al. described that the use of a dominant negative Drp1 strategy rescues insulin signaling after palmitate treatment in skeletal muscle cells (19), thus emphasizing the importance of mitochondrial network integrity. In accord with these findings, our data revealed no impact of Drp1K38A on insulin response, indicating that, while a certain amount of mitochondrial fusion is necessary for this pathway, other components may also act as limiting steps. In this way, our data show that dominant negative Drp1 alone does not enhance glucose uptake in response to insulin, but the above-mentioned study shows that Drp1K38A or short hairpin Drp1 can reverse insulin resistance induced by palmitate, since it causes via mitochondrial fragmentation (19).

The relevance of the changes in mitochondrial morphology could be associated with their direct effect on Ca^{2+} homeostasis. Mitochondria are dynamic Ca^{2+} regulators capable of rapid uptake from domains of high concentration. This way, they act as buffers, taking up Ca^{2+} especially at releasing sites on the ER surface and therefore preventing a prolonged rise in cytosolic concentration (16). According to our data, the size of individual mitochondria affects their Ca^{2+} buffering capacity, thus modulating both mitochondrial and cytosolic Ca^{2+} availability. Previous findings from our laboratory showed that Ca^{2+} entry into the mitochondrial matrix is required for energy production in a stressed condition (7). In this work, we tested mitochondrial morphology as a modulator of Ca^{2+} homeostasis in response to insulin. We show here for the first time that insulin promotes Ca^{2+} transfer into mitochondria of skeletal muscle cells. This process greatly depends on mitochondrial morphology, since it is significantly diminished after Mfn2 or Opa1 silencing. To further investigate the impact of mitochondrial Ca^{2+} uptake on insulin signaling, we used the mitochondrial Ca^{2+} uniporter inhibitor RuRed, resulting in both diminished Akt at Ser^{473} phosphorylation and GLUT4 exofacial exposure. On the basis of these findings, we conclude that mitochondrial morphology itself can modulate insulin metabolic stimulation, where mitochondria Ca^{2+} uptake seems to

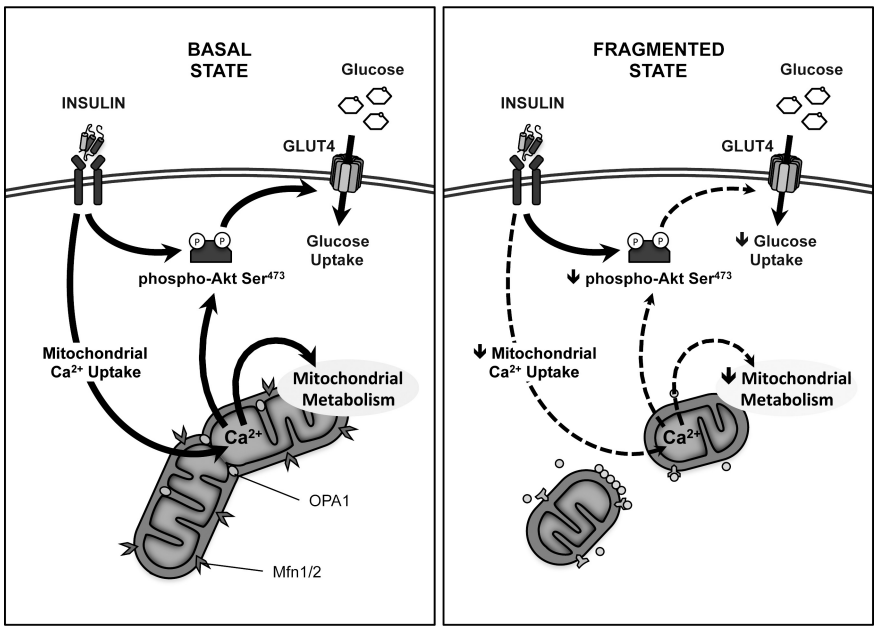

Fig. 10. Proposed mechanism for the role of mitochondrial dynamics in insulin signaling. *Left*: in an interconnected mitochondrial network, insulin induces a rise in mitochondrial Ca^{2+} uptake, which is key for the full activation of Akt and downstream glucose uptake. *Right*: in contrast, in a fragmented mitochondrial network, the insulin-induced mitochondrial Ca^{2+} signal is impaired, with a subsequent decrease in Akt activation and glucose uptake.

have a key role in Akt Ser^{473} phosphorylation and glucose uptake in response to insulin.

The relationship between mitochondrial dynamics and Ca^{2+} signaling is, in fact, complex, as they are constantly giving shape to each other. Aside from energy production, Ca^{2+} modulates mitochondrial mobility along cytoskeleton tubules (21) as well as mitochondrial fragmentation via Drp1 (13). Both of these properties, in turn, determine mitochondrial buffering capacity, thus regulating intracellular Ca^{2+} levels. Additionally, Ca^{2+} regulates lysosome-mediated mitochondrial degradation, termed mitophagy. This process is known to require a mitochondrial fusion/fission balance to produce mitochondria small enough to be subject to degradation (33). Mitophagy is the basis of mitochondrial quality control and therefore crucial for maintaining a fully functional network. To address the possible participation of this process in our model, we tested whether our experimental strategies stimulate mitophagy. Both AsMfn2 and RuRed treatments increased lysosome-mitochondria colocalization and led to accumulation of the mitophagy-promoting kinase PINK1, compared with untreated cells (Fig. 9). This observation suggests that impaired mitochondrial Ca^{2+} uptake, either via disruption of the network continuity or via blockade of the uniporter, leads to mitochondrial deterioration and thereby to increased turnover. Lowering the quality of the mitochondrial network might contribute to the decreased insulin response, not only at the energy production level but also leading to signaling alterations.

All together, our findings show that mitochondrial morphology is an important regulator of mitochondrial Ca^{2+} uptake, likely through modulation of diffusion across different parts of the network. This aspect of mitochondrial dynamics is important for insulin signaling, as impaired Ca^{2+} entry into the mitochondrial matrix significantly compromises Akt activation and its downstream effects. Mitochondrial fragmentation, but not elongation, affected Akt activation and energy production in response to insulin. The presence of mitophagy in this scenario strongly suggests that maintenance of network continuity is necessary for mitochondrial function in response to stimuli. In consequence, the present work shows for the first time that control of mitochondrial Ca^{2+} uptake through mitochondrial morphology is a critical step for insulin-induced Akt-dependent glucose uptake (Fig. 10).

ACKNOWLEDGMENTS

We thank Dr. Antonio Zorzano (Institute of Research in Biomedicine, Barcelona, Spain) for the kind donation of AsMfn2 and Drp1K38A adenoviruses and miRNA for Opa1. The L6-GLUT4myc (L6) cell line was kindly donated by Dr. Amira Klip (Division of Cell Biology, Hospital for Sick Children, Toronto, ON, Canada). We also thank Fidel Albornoz for excellent technical assistance.

GRANTS

This work was supported by FONDECYT (Grant 1120212 to S. Lavandero, 3110114 to R. Troncoso, 1110180 to M. Chiong, and 3110170 to A. Contreras-Ferrat), CONICYT (Grant Anillo ACT1111 to S. Lavandero and M. Chiong), and FONDAP (Grant 15130011 to S. Lavandero). We are thankful for the PhD and MSc fellowships from CONICYT Chile to A. del Campo, V. Parra, H. E. Verdejo, P. E. Morales, R. Bravo-Sagua, M. F. Navarro-Marquez, and C. López-Crisosto. V. Parra holds a postdoctoral international fellowship from Bicentennial Program, CONICYT, Chile.

DISCLOSURES

No conflicts of interest, financial or otherwise, are declared by the author(s).

AUTHOR CONTRIBUTIONS

Author contributions: A.d.C., R.T., M.C., and S.L. conception and design of research; A.d.C., V.P., C.V.-T., T.G., P.E.M., C.L.-C., R.B.-S., M.F.N.-M., and A.C.-F. performed experiments; A.d.C., V.P., C.V.-T., T.G., P.E.M., C.L.-C., R.B.-S., M.F.N.-M., H.E.V., A.C.-F., R.T., M.C., and S.L. analyzed data; A.d.C., C.L.-C., R.B.-S., M.F.N.-M., H.E.V., A.C.-F., R.T., M.C., and S.L. interpreted results of experiments; A.d.C., R.T., M.C., and S.L. drafted manuscript; A.d.C., H.E.V., R.T., M.C., and S.L. edited and revised manuscript; A.d.C., V.P., C.V.-T., T.G., P.E.M., R.B.-S., M.F.N.-M., H.E.V., A.C.-F., R.T., M.C., and S.L. approved final version of manuscript; P.E.M. and M.C. prepared figures.

REFERENCES

1. **Bach D, Naon D, Pich S, Soriano FX, Vega N, Rieusset J, Laville M, Guillet C, Boirie Y, Wallberg-Henriksson H, Manco M, Calvani M, Castagneto M, Palacin M, Mingrone G, Zierath JR, Vidal H, Zorzano A.** Expression of Mfn2, the Charcot-Marie-Tooth neuropathy type 2A gene, in human skeletal muscle: effects of type 2 diabetes, obesity, weight loss, and the regulatory role of tumor necrosis factor alpha and interleukin-6. *Diabetes* 54: 2685–2693, 2005.
2. **Bach D, Pich S, Soriano FX, Vega N, Baumgartner B, Oriola J, Daugaard JR, Lloberas J, Camps M, Zierath JR, Rabasa-Lhoret R, Wallberg-Henriksson H, Laville M, Palacin M, Vidal H, Rivera F, Brand M, Zorzano A.** Mitofusin-2 determines mitochondrial network architecture and mitochondrial metabolism. A novel regulatory mechanism altered in obesity. *J Biol Chem* 278: 17190–17197, 2003.
3. **Belenguer P, Pellegrini L.** The dynamin GTPase OPA1: more than mitochondria? *Biochim Biophys Acta* 1833: 176–183, 2013.
4. **Benard G, Bellance N, Jose C, Melser S, Nouette-Gaulain K, Rossignol R.** Multi-site control and regulation of mitochondrial energy production. *Biochim Biophys Acta* 1797: 698–709, 2010.
5. **Benard G, Rossignol R.** Mitochondrial fluidity matters. Focus on "Inherited complex I deficiency is associated with faster protein diffusion in the matrix of moving mitochondria." *Am J Physiol Cell Physiol* 294: C1123–C1130, 2008.
6. **Betz C, Stracka D, Prescianotto-Baschong C, Frieden M, Demaurex N, Hall MN.** Feature Article: mTOR complex 2-Akt signaling at mitochondria-associated endoplasmic reticulum membranes (MAM) regulates mitochondrial physiology. *Proc Natl Acad Sci USA* 110: 12526–12534, 2013.
7. **Bravo R, Gutierrez T, Paredes F, Gatica D, Rodriguez AE, Pedrozo Z, Chiong M, Parra V, Quest AF, Rothermel BA, Lavandero S.** Endoplasmic reticulum: ER stress regulates mitochondrial bioenergetics. *Int J Biochem Cell Biol* 44: 16–20, 2012.
8. **Bravo R, Vicencio JM, Parra V, Troncoso R, Munoz JP, Bui M, Quiroga C, Rodriguez AE, Verdejo HE, Ferreira J, Iglewski M, Chiong M, Simmen T, Zorzano A, Hill JA, Rothermel BA, Szabadkai G, Lavandero S.** Increased ER-mitochondrial coupling promotes mitochondrial respiration and bioenergetics during early phases of ER stress. *J Cell Sci* 124: 2143–2152, 2011.
9. **Brown GC.** Control of respiration and ATP synthesis in mammalian mitochondria and cells. *Biochem J* 284: 1–13, 1992.
10. **Cardenas C, Foskett JK.** Mitochondrial Ca(2+) signals in autophagy. *Cell Calcium* 52: 44–51, 2012.
11. **Chen L, Gong Q, Stice JP, Knowlton AA.** Mitochondrial OPA1, apoptosis, and heart failure. *Cardiovasc Res* 84: 91–99, 2009.
12. **Contreras-Ferrat AE, Toro B, Bravo R, Parra V, Vasquez C, Ibarra C, Mears D, Chiong M, Jaimovich E, Klip A, Lavandero S.** An inositol 1,4,5-triphosphate (IP3)-IP3 receptor pathway is required for insulin-stimulated glucose transporter 4 translocation and glucose uptake in cardiomyocytes. *Endocrinology* 151: 4665–4677, 2010.
13. **Cribbs JT, Strack S.** Reversible phosphorylation of Drp1 by cyclic AMP-dependent protein kinase and calcineurin regulates mitochondrial fission and cell death. *EMBO Rep* 8: 939–944, 2007.
14. **de Brito OM, Scorrano L.** Mitofusin 2 tethers endoplasmic reticulum to mitochondria. *Nature* 456: 605–610, 2008.
15. **Escobar-Henriques M, Anton F.** Mechanistic perspective of mitochondrial fusion: tubulation vs. fragmentation. *Biochim Biophys Acta* 1833: 162–175, 2013.
16. **Grimm S.** The ER-mitochondria interface: the social network of cell death. *Biochim Biophys Acta* 1823: 327–334, 2012.
17. **Hernandez-Alvarez MI, Thabit H, Burns N, Shah S, Brema I, Hatunic M, Finucane F, Liesa M, Chiellini C, Naon D, Zorzano A, Nolan JJ.**

Subjects with early-onset type 2 diabetes show defective activation of the skeletal muscle PGC-1(alpha)/Mitofusin-2 regulatory pathway in response to physical activity. *Diabetes Care* 33: 645–651, 2010.

18. **JeBailey L, Rudich A, Huang X, Di Ciano-Oliveira C, Kapus A, and Klip A.** Skeletal muscle cells and adipocytes differ in their reliance on TC10 and Rac for insulin-induced actin remodeling. *Mol Endocrinol* 18: 359–372, 2004.
19. **Jheng HF, Tsai PJ, Guo SM, Kuo LH, Chang CS, Su IJ, Chang CR, Tsai YS.** Mitochondrial fission contributes to mitochondrial dysfunction and insulin resistance in skeletal muscle. *Mol Cell Biol* 32: 309–319, 2012.
20. **Kelley DE, He J, Menshikova EV, Ritov VB.** Dysfunction of mitochondria in human skeletal muscle in type 2 diabetes. *Diabetes* 51: 2944–2950, 2002.
21. **Liu X, Hajnoczky G.** Ca2+-dependent regulation of mitochondrial dynamics by the Miro-Milton complex. *Int J Biochem Cell Biol* 41: 1972–1976, 2009.
22. **Marambio P, Toro B, Sanhueza C, Troncoso R, Parra V, Verdejo H, Garcia L, Quiroga C, Munafo D, Diaz-Elizondo J, Bravo R, Gonzalez MJ, Diaz-Araya G, Pedrozo Z, Chiong M, Colombo MI, Lavandero S.** Glucose deprivation causes oxidative stress and stimulates aggresome formation and autophagy in cultured cardiac myocytes. *Biochim Biophys Acta* 1802: 509–518, 2010.
23. **Munoz JP, Chiong M, Garcia L, Troncoso R, Toro B, Pedrozo Z, Diaz-Elizondo J, Salas D, Parra V, Nunez MT, Hidalgo C, Lavandero S.** Iron induces protection and necrosis in cultured cardiomyocytes: role of reactive oxygen species and nitric oxide. *Free Radic Biol Med* 48: 526–534, 2010.
24. **Munoz JP, Ivanova S, Sanchez-Wandelmer J, Martinez-Cristobal P, Noguera E, Sancho A, Diaz-Ramos A, Hernandez-Alvarez MI, Sebastian D, Mauvezin C, Palacin M, Zorzano A.** Mfn2 modulates the UPR and mitochondrial function via repression of PERK. *EMBO J* 32: 2348–2361, 2013.
25. **Parra V, Eisner V, Chiong M, Criollo A, Moraga F, Garcia A, Hartel S, Jaimovich E, Zorzano A, Hidalgo C, Lavandero S.** Changes in mitochondrial dynamics during ceramide-induced cardiomyocyte early apoptosis. *Cardiovasc Res* 77: 387–397, 2008.
26. **Pfaffenbach KT, Lee AS.** The critical role of GRP78 in physiologic and pathologic stress. *Curr Opin Cell Biol* 23: 150–156, 2011.
27. **Quiros PM, Ramsay AJ, Sala D, Fernandez-Vizarra E, Rodriguez F, Peinado JR, Fernandez-Garcia MS, Vega JA, Enriquez JA, Zorzano A, Lopez-Otin C.** Loss of mitochondrial protease OMA1 alters processing of the GTPase OPA1 and causes obesity and defective thermogenesis in mice. *EMBO J* 31: 2117–2133, 2012.
28. **Rudich A, Klip A.** Push/pull mechanisms of GLUT4 traffic in muscle cells. *Acta Physiol Scand* 178: 297–308, 2003.
29. **Sarbassov DD, Guertin DA, Ali SM, Sabatini DM.** Phosphorylation and regulation of Akt/PKB by the rictor-mTOR complex. *Science* 307: 1098–1101, 2005.
30. **Sebastian D, Hernandez-Alvarez MI, Segales J, Sorianello E, Munoz JP, Sala D, Waget A, Liesa M, Paz JC, Gopalacharyulu P, Oresic M, Pich S, Burcelin R, Palacin M, Zorzano A.** Mitofusin 2 (Mfn2) links mitochondrial and endoplasmic reticulum function with insulin signaling and is essential for normal glucose homeostasis. *Proc Natl Acad Sci USA* 109: 5523–5528, 2012.
31. **Segales J, Paz JC, Hernandez-Alvarez MI, Sala D, Munoz JP, Noguera E, Pich S, Palacin M, Enriquez JA, Zorzano A.** A form of mitofusin 2 (Mfn2) lacking the transmembrane domains and the COOH-terminal end stimulates metabolism in muscle and liver cells. *Am J Physiol Endocrinol Metab* 304: E1208–E1221, 2013.
32. **Troncoso R, Vicencio JM, Parra V, Nemchenko A, Kawashima Y, Del Campo A, Toro B, Battiprolu PK, Aranguiz P, Chiong M, Yakar S, Gillette TG, Hill JA, Abel ED, Leroith D, Lavandero S.** Energy-preserving effects of IGF-1 antagonize starvation-induced cardiac autophagy. *Cardiovasc Res* 93: 320–329, 2012.
33. **Twig G, Elorza A, Molina AJ, Mohamed H, Wikstrom JD, Walzer G, Stiles L, Haigh SE, Katz S, Las G, Alroy J, Wu M, Py BF, Yuan J, Deeney JT, Corkey BE, Shirihai OS.** Fission and selective fusion govern mitochondrial segregation and elimination by autophagy. *EMBO J* 27: 433–446, 2008.
34. **Verdejo HE, Del Campo A, Troncoso R, Gutierrez T, Toro B, Quiroga C, Pedrozo Z, Munoz JP, Garcia L, Castro PF, Lavandero S.** Mitochondria, myocardial remodeling, and cardiovascular disease. *Curr Hypertens Rep* 14: 532–539, 2012.
35. **Walder K, Kerr-Bayles L, Civitarese A, Jowett J, Curran J, Elliott K, Trevaskis J, Bishara N, Zimmet P, Mandarino L, Ravussin E, Blangero J, Kissebah A, Collier GR.** The mitochondrial rhomboid protease PSARL is a new candidate gene for type 2 diabetes. *Diabetologia* 48: 459–468, 2005.
36. **Wang Q, Khayat Z, Kishi K, Ebina Y, Klip A.** GLUT4 translocation by insulin in intact muscle cells: detection by a fast and quantitative assay. *FEBS Lett* 427: 193–197, 1998.
37. **Zorzano A, Hernandez-Alvarez MI, Palacin M, Mingrone G.** Alterations in the mitochondrial regulatory pathways constituted by the nuclear co-factors PGC-1alpha or PGC-1beta and mitofusin 2 in skeletal muscle in type 2 diabetes. *Biochim Biophys Acta* 1797: 1028–1033, 2010.